Acta Crystallographica Section D
Biological Crystallography
ISSN 0907-4449

Revisiting the *Haloarcula marismortui* 50S ribosomal subunit model

Azat Gabdulkhakov,* Stanislav Nikonov and Maria Garber

Institute of Protein Research, RAS, Pushchino, Moscow Region 142290, Russian Federation

Correspondence e-mail: azat@vega.protres.ru

Received 1 December 2012
Accepted 18 February 2013

PDB References:
H. marismortui large ribosomal subunit, 4hub; 4i4m

The structure of the large ribosomal subunit from the halophilic archaeon *Haloarcula marismortui* (Hma) is the only crystal structure of an archaeal ribosomal particle that has been determined to date. However, the first model of the Hma 50S ribosomal subunit contained some gaps: the structures of functionally important mobile lateral protuberances were not visualized. Subsequently, some parts of the P (L12) stalk base were visualized at 3.0 Å resolution [Kavran & Steitz (2007), *J. Mol. Biol.* **371**, 1047–1059]: the RNA-binding domain of r-protein P0 (L10), the C-terminal domain of L11 and helices 43 and 44 of the 23 S rRNA. Here, the 2.4 Å resolution electron-density map of the Hma 50S ribosomal subunit was revisited and approximately two-thirds of the P0 protein, residues 1–58 of the N-terminal domains of two P1 protein molecules, residues 130–156 of L11, the full-length r-protein LX, nucleotides 2137–2149 and 2226–2237 of the 23S rRNA helix H76 forming the L1 stalk, nucleotides 2339–2343 of the 23S rRNA (contacting L5 protein) and loops 29–34 and 108–128 of protein L5 could be visualized. Thus, this paper provides a supplemented version of the Hma 50S ribosomal subunit model.

1. Introduction

The 2.4 Å resolution structure of the *Haloarcula marismortui* (Hma) large ribosomal subunit appeared 12 years ago and is the highest resolution structure of a ribosomal particle that has been obtained to date (Ban *et al.*, 2000). Unfortunately, not all elements of the 50S ribosomal subunit structure could be identified and included in the model. First of all, the lateral ribosomal protuberances L1 and P (L12) were not visualized. The P (L12) stalk is involved in the formation of the so-called 'GTPase-associated site' and plays a key role in the interaction of the ribosome with GTP-bound translation factors and in the control of translation accuracy (Möller & Maassen, 1986; Diaconu *et al.*, 2005). Later, Kavran and Steitz were able to find conditions that resulted in a more ordered P stalk in the Hma large ribosomal subunit crystals and consequently allowed the visualization of approximately 80% of L11, the RNA-binding domain of P0 and helices 43 and 44 of the 23S rRNA (Kavran & Steitz, 2007).

The archaeal counterpart of the bacterial ribosomal protein (r-protein) L10 is presently called P0 because of its high similarity to its eukaryotic homologue (called P0), and the entire lateral ribosomal stalk of the archaeal ribosome (analogous to the L12 stalk in bacteria) is now named the P stalk for the same reason. Archaeal P1 and eukaryotic P1/P2 proteins are much shorter than their bacterial counterpart L12, whereas archaeal/eukaryotic P0 is much longer than the bacterial L10 and contains a specific insertion within the

N-terminal domain and a C-terminal extension. The structure of the N-terminal RNA-binding domain of P0 and L10 is universally conserved in eukarya, archaea and bacteria. This conservation allows the *in vitro* replacement of the L10–L7/L12 complex in the *Escherichia coli* 50S ribosomal subunit by the archaeal P0–P1 complex or the eukaryotic P0–P1/P2 complex. Such chimeric ribosomes recruited archaeal and eukaryotic elongation factors but were inactive with bacterial factors (Nomura *et al.*, 2006; Uchiumi *et al.*, 2002).

Recently, progress has been made in structural studies of the isolated components of the L12 stalk of bacterial ribosomes and the P stalk of archaeal ribosomes (Diaconu *et al.*, 2005; Naganuma *et al.*, 2010). In 2010, the structure of a two-domain N-terminal fragment of *Methanococcus jannaschii* r-protein P0 (MjaL10NTF) was determined at 1.6 Å resolution (Kravchenko *et al.*, 2010). This structure contains the strongly conserved RNA-binding domain and the second domain, which corresponds to a specific insertion (about 70 amino-acid residues) in the sequences of archaeal and eukaryotic P0 r-proteins. The second domain is linked to the RNA-binding domain through a flexible hinge and can move and change its relative position within the two-domain structure; the structure of the insertion domain is unique and was described for the first time in the work of Kravchenko *et al.* (2010).

Table 1
Refinement statistics for the Hma 50S ribosomal subunit.

Values in parentheses are for the highest resolution shell.

Space group	$C222_1$
Unit-cell parameters (Å)	a = 211.66, b = 299.67, c = 573.77
Resolution (Å)	85.53–2.40 (2.43–2.40)
No. of reflections	666777 (15697)
R factor (%)	16.56 (27.7)
Free R factor (%)	20.62 (31.9)
Overall B factor (Å^2)	21.3
R.m.s. deviations	
Bond lengths (Å)	0.006
Bond angles (°)	1.078
Ramachandran plot (%)	
Most favoured	92.5
Additionally allowed	6.7
Generously allowed	0.6
Disallowed	0.2

The next functionally important region of the ribosome is the L1 stalk. The L1 protuberance of the 50S ribosomal subunit is implicated in the release/disposal of deacylated tRNA from the E site. In the 23S rRNA, L1 protects helices 76, 77 and 78 and the loops that interconnect them from nuclease attack (Zimmermann, 1980). For a long time, the high mobility of this ribosomal domain prevented accurate determination of its three-dimensional structure within the ribosomal particles. The binding of EF-G trapped in the post-translocational state by the antibiotic fusidic acid contributed to the stabilization of the mobile elements of the ribosome and

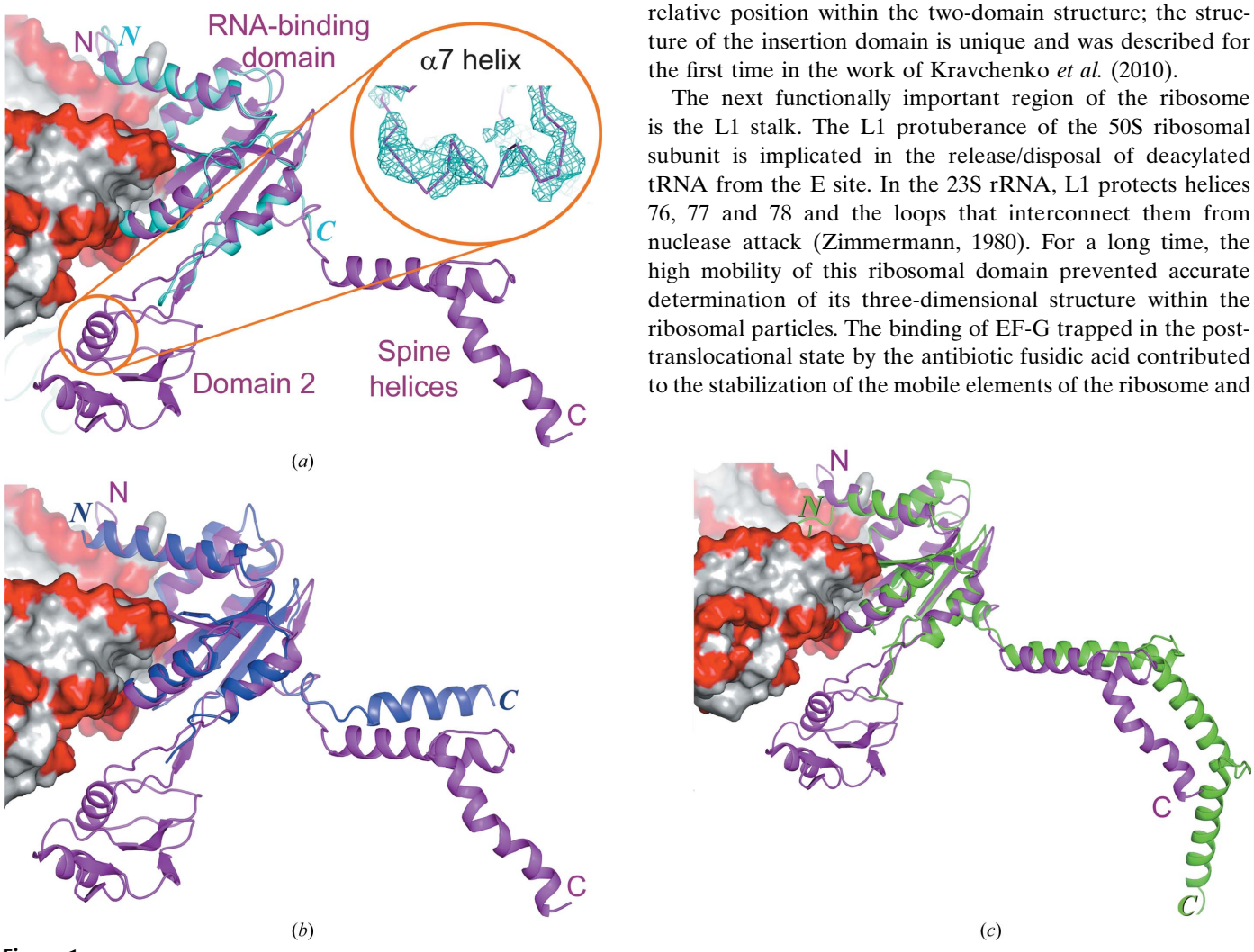

Figure 1
Superposition of the P-stalk region of the presented Hma large ribosomal subunit structure (magenta) (*a*) on the previous model of this ribosomal subunit (PDB entry 2qa4; Kavran & Steitz, 2007; r-protein P0 in cyan); the α7 helix (amino acids 171–182) of the obtained model is shown in an orange circle and magnified with unbiased electron density at the 1.0σ level; (*b*) on the P0 protein (blue) in the *S. cerevisiae* ribosome structure (PDB entry 3u5h; Ben-Shem *et al.*, 2011); (*c*) on the structure of the isolated P0 (green) from *P. horikoshii* (PDB entry 3a1y; Naganuma *et al.*, 2010). In all cases the N-terminal domains of P0 were superimposed.

allowed a more complete model of the *Thermus thermophilus* ribosome that included the entire L1 stalk to be built at 3.6 Å resolution (Gao *et al.*, 2009).

In the present work, the incorporation of domain 2 of r-protein P0 into the available density in a 2.4 Å resolution map of Hma 50S (PDB entry 1ffk; Ban *et al.*, 2000) and refinement were performed. This led to the possibility of finding and interpreting the density for approximately two-thirds of P0 (211 complete amino-acid residues and 49 residues as a polyalanine chain) and for a dimer of the N-terminal domain (NTD) of P1 (as a polyalanine chain). Step-by-step multiple refinement led to the visualization of some of the other ribosomal components: the C-terminal part of r-protein L11 (residues 131–156), r-protein LX, nucleotides 2339–2343 of the 23S rRNA contacting the L5 protein and loops 29–34 and 108–128 of L5 and nucleotides 2137–2149 and 2226–2237 of the 23S rRNA H76, which belongs to the L1 stalk.

2. Materials and methods

The refined crystal structure of the *H. marismortui* large ribosomal subunit at 2.4 Å resolution with the rRNA sequence of the 23S rRNA and genome-derived sequences of r-proteins (PDB entry 3cc2; Blaha *et al.*, 2008) was used as the starting model. The structure factors were taken from the first structure of the large ribosomal subunit at 2.4 Å resolution (PDB entry 1ffk; Ban *et al.*, 2000). The initial model was subjected to crystallographic refinement, initially with *REFMAC5* (Murshudov *et al.*, 2011; the initial R factor was 19.21% and the initial $R_{\rm free}$ was 22.70%) and subsequently with *PHENIX* (Afonine *et al.*, 2012). Manual rebuilding of the model was carried out in *Coot* (Emsley *et al.*, 2010). The final model of the Hma 50S ribosomal subunit, which was refined to an R factor of 16.56% and an $R_{\rm free}$ of 20.62% at 2.4 Å resolution, includes 2808 nucleotides of the 2922 in the 23S RNA, all of the 122 nucleotides in the 5S RNA and 4311 amino-acid residues from 32 ribosomal proteins, as well as 261 ions (138 Mg^{2+}, 30 Cl^{-}, 85 Na^{+}, three K^{+} and five Cd^{2+} ions) and 7745 water molecules. The quality of the model was checked using *PROCHECK* (Laskowski *et al.*, 1993) and *WHAT_CHECK* (Hooft *et al.*, 1996), and showed that 92.5% of the residues have the most favoured conformations, while the remainder are in additionally allowed regions. Refinement statistics are summarized in Table 1. The atomic coordinates have been deposited in the RCSB Protein Data Bank and are available under accession codes 4hub and 4i4m. Figures were prepared using *PyMOL* (http://www.pymol.org).

3. Results

3.1. Ribosomal protein P0

The structure of the second domain of MjaL10NTF (Kravchenko *et al.*, 2010) was incorporated into the 2.4 Å resolution electron-density map of the Hma 50S ribosomal subunit at the 1.0σ level downloaded from the PDB by *Coot* (Emsley *et al.*, 2010). The best piece of density was found for

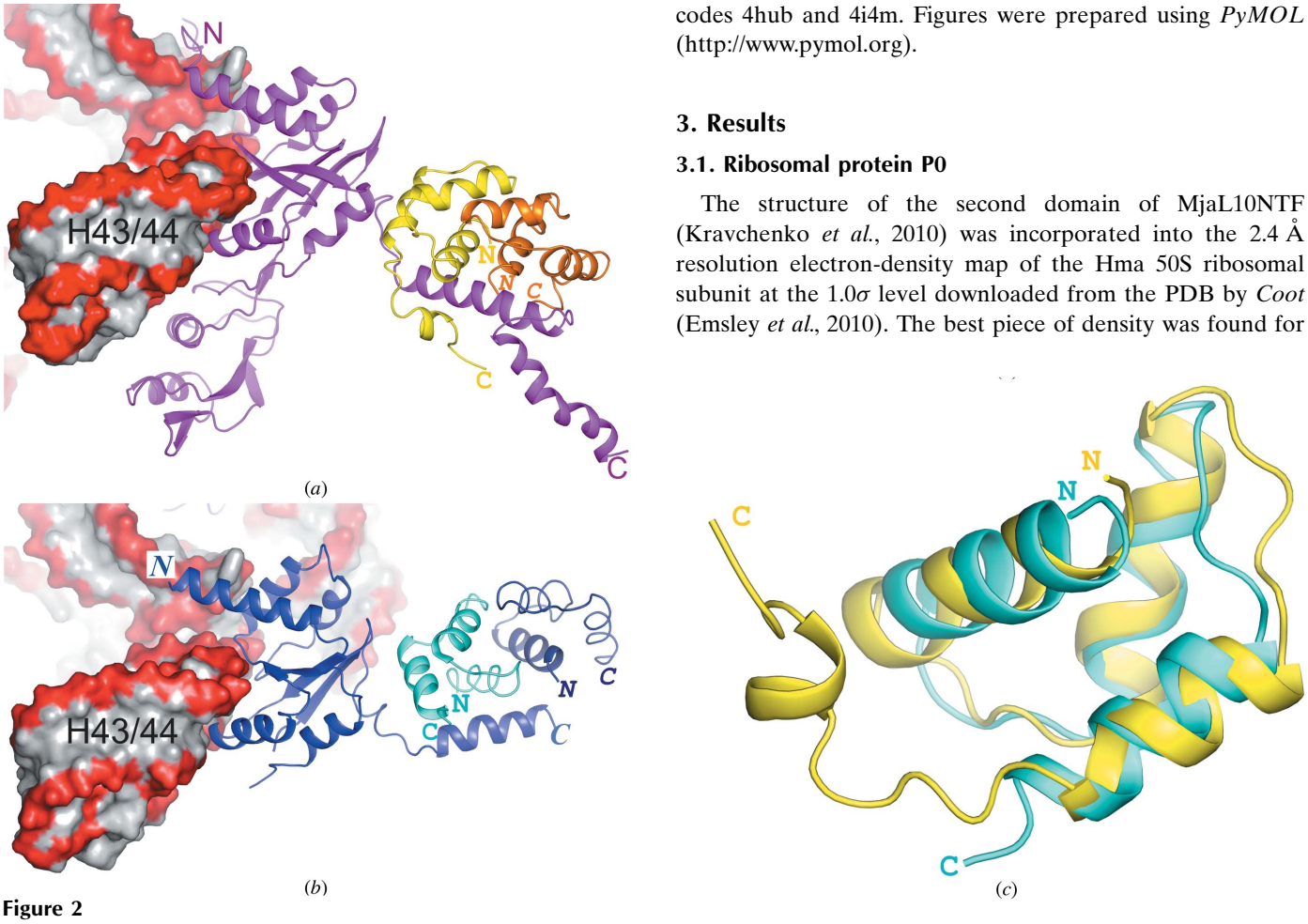

Figure 2
The P1 NTD dimer structure (as a polyalanine chain) in models of the Hma and *S. cerevisiae* ribosomes. (*a*) The present Hma large ribosomal subunit structure in the region of the P stalk (P0, magenta; two copies of the NTD of P1, yellow and orange). (*b*) The same region of the *S. cerevisiae* ribosome (P0, blue; P1 α, cyan; P1 β, deep blue). (*c*) Superposition of the first P1 NTD monomer (yellow) in the present Hma large ribosomal subunit model on the P1 α NTD (cyan) from the *S. cerevisiae* ribosome model.

helix α7 (Fig. 1*a*) and this finding helped to orientate the whole structure of domain 2 (the insertion domain) of P0 within the archaeal ribosomal subunit. Moreover, in the process of structure refinement we could interpret density for the helices belonging to the C-terminal part of the P0 protein. Superpositions of the obtained Hma large ribosomal subunit structure in the P0 region on the available model of this ribosomal subunit (PDB entry 2qa4; Kavran & Steitz, 2007) and on the P0 protein in the *Saccharomyces cerevisiae* ribosome structure (PDB entry 3u5h; Ben-Shem *et al.*, 2011) are shown in Figs. 1(*a*) and 1(*b*), respectively. Fig. 1(*c*) shows a superposition of the obtained structure on the structure of the isolated P0 protein from the archaeon *Pyrococcus horikoshii* (PDB entry 3a1y; Naganuma *et al.*, 2010). In all cases there is a good coincidence for domain 1 of the proteins, but domain 2 is present only in the obtained structure (in the structure of the isolated *P. horikoshii* P0 this domain was described as disordered).

Domain 2 of Hma P0 is located on the outer side of the ribosome body between the C-terminal domain of L6, the N-terminal domain of L11 and the H42–H44 region of the 23S rRNA. However, this domain only contacts the N-terminal domain of r-protein L11 and forms one hydrogen bond (the contact area is 100 Å^2, which is equal to 0.7% of the total surface of protein P0). The surface of domain 2, especially the top with the flat hydrophobic patch and β-sheet regions, is accessible to interactions with other components of the translation system, apparently with translation factors.

Previously, structures of full-length bacterial L10 and incomplete archaeal P0 (without domain 2) have been determined in complexes with NTD dimers of L12 or P1 proteins, respectively (Diaconu *et al.*, 2005; Naganuma *et al.*, 2010). L10 and P0 have a similar domain organization: the conserved RNA-binding domain (with the insertion domain in archaea) is followed by the C-terminal spine helices to which L12 or P1 dimers bind. In contrast to the structural similarity of the strongly conserved RNA-binding domains, the helical spines have different structural characteristics in bacterial L10 and archaeal P0. In L10, the spine consists of one curved helix with two kinks; the archaeal spine is composed of three independent α-helices connected by short linkers (Naganuma *et al.*, 2010). Each of these α-helices of the P0 spine is associated with one P1 dimer.

The majority of the L12 stalk was visualized within the bacterial ribosome crystallized in complex with elongation factor G (Gao *et al.*, 2009). The components of the eukaryotic ribosomal P stalk were partially visualized in the structure of the 80S ribosome (Ben-Shem *et al.*, 2011).

Here, we were able to visualize some components of the archaeal P stalk, including the insertion domain of P0 (using the structure of MjaL10NTF as the model) and two spine helices (using the structure of the isolated *P. horikoshii* P0 as the model). However, while the RNA-binding domain of Hma P0 and the insertion domain are visible in the high-resolution map, the spine helices 1 and 2 could only be placed as poly-alanine chains (Fig. 1).

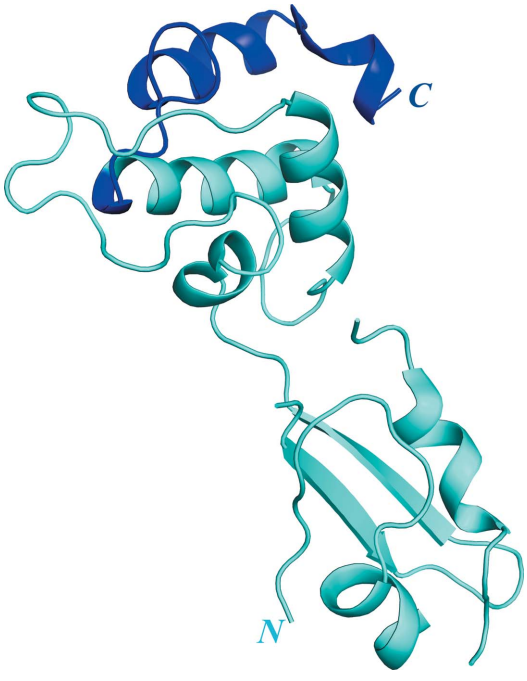

Figure 3
The supplemented structure of Hma r-protein L11 (the previously determined part is shown in cyan and the supplemental C-terminal part is shown in dark blue).

3.2. Ribosomal protein P1

Spine helix 1 of Hma P0 was visualized as the helix bound to the P1 NTD dimer. As a model for the P1 structure, we used the structure of the P1 NTD from *P. horikoshii* (PDB entry 3a1y; Naganuma *et al.*, 2010; Fig. 2*a*).

Archaeal P1 and eukaryotic P1/P2 share no sequence similarity with their bacterial counterpart L12, and the tertiary structures of these proteins are also unrelated (Naganuma *et al.*, 2010). Despite the lack of an evolutionary relationship, the archaeal/eukaryotic and bacterial proteins have a similar domain organization, but their domains have very different sizes. The tertiary structure of the P1 NTD dimer from the *S. cerevisiae* ribosome was described for the first time by Ben-Shem *et al.* (2011) (Fig. 2*b*). Comparison of the structures of the NTDs of eukaryotic and archaeal P1 proteins shows that their tertiary structures are very similar (Fig. 2*c*).

3.3. Ribosomal protein L11

Ribosomal proteins P0 (L10) and L11 simultaneously bind to a platform on helices 43 and 44 (H43/44) of the 23S rRNA. These r-proteins form the base of the P (L12) stalk and are involved in its function. Previous models of the Hma 50S ribosomal subunit included the N-terminal (residues 3–70) and the C-terminal (residues 71–129) domains of r-protein L11. We were now able to find and interpret density for the most distal part of the C-terminal domain of this protein: residues 130–156 (Fig. 3). Unfortunately, we were not able to find density for the regions 25–27 and 44–48 of the NTD (the latter is located near the hinge connecting the two domains).

3.4. Ribosomal protein LX

Refinement of the Hma 50S structure led to the finding of density between the central protuberance (CP) and the P stalk (Figs. 4*a* and 4*c*). A polyalanine model of the protein was built and a structural homology search was performed using the *DALI* server (Holm & Rosenström, 2010).

Maximal homology was found to r-protein LX from the archaeon *Methanothermobacter thermautotrophicus*, which was solved by the Northeast Structural Genomics Consortium (NESG) and used in the cryo-EM structure of the 50S ribosomal subunit from *M. thermautotrophicus* (Greber *et al.*, 2012); the C-terminal domains of r-proteins L20e from the *S. cerevisiae* ribosome (PDB entry 3u5e; Ben-Shem *et al.*, 2011) and L18Ae from the *Tetrahymena thermophila* ribosome (PDB entry 4a19; Klinge *et al.*, 2011) also demonstrated good homology with our model. The gene for the LX protein is present in the *H. marismortui* genome, but this protein was not included in the X-ray crystal structure of the 50S ribosomal subunit from this organism (Ban *et al.*, 2000). In the recently published 6.6 Å resolution cryo-EM structure of the 50S ribosomal subunit from the archaeon *M. thermautotrophicus* LX is present (Mth LX; Greber *et al.*, 2012). Hma LX (57 amino acids) is shorter than Mth LX (78 amino acids). These proteins demonstrate 30% identity and 45% homology. Fig. 4(*d*) shows a superposition of these two proteins located in the models of the Hma and *M. thermautotrophicus* 50S ribosomal subunits, correspondingly.

The LX protein contacts the 23S rRNA in a cavity between two helices in the region of nucleotides 1112–1115, 1252–1250, 1141–1143, 1224–1223 and the top of loop 578 (Fig. 4*a*). The protein forms 21 hydrogen bonds to rRNA, but only three of them are nucleotide-specific (Fig. 4*b*). A hydrophobic effect

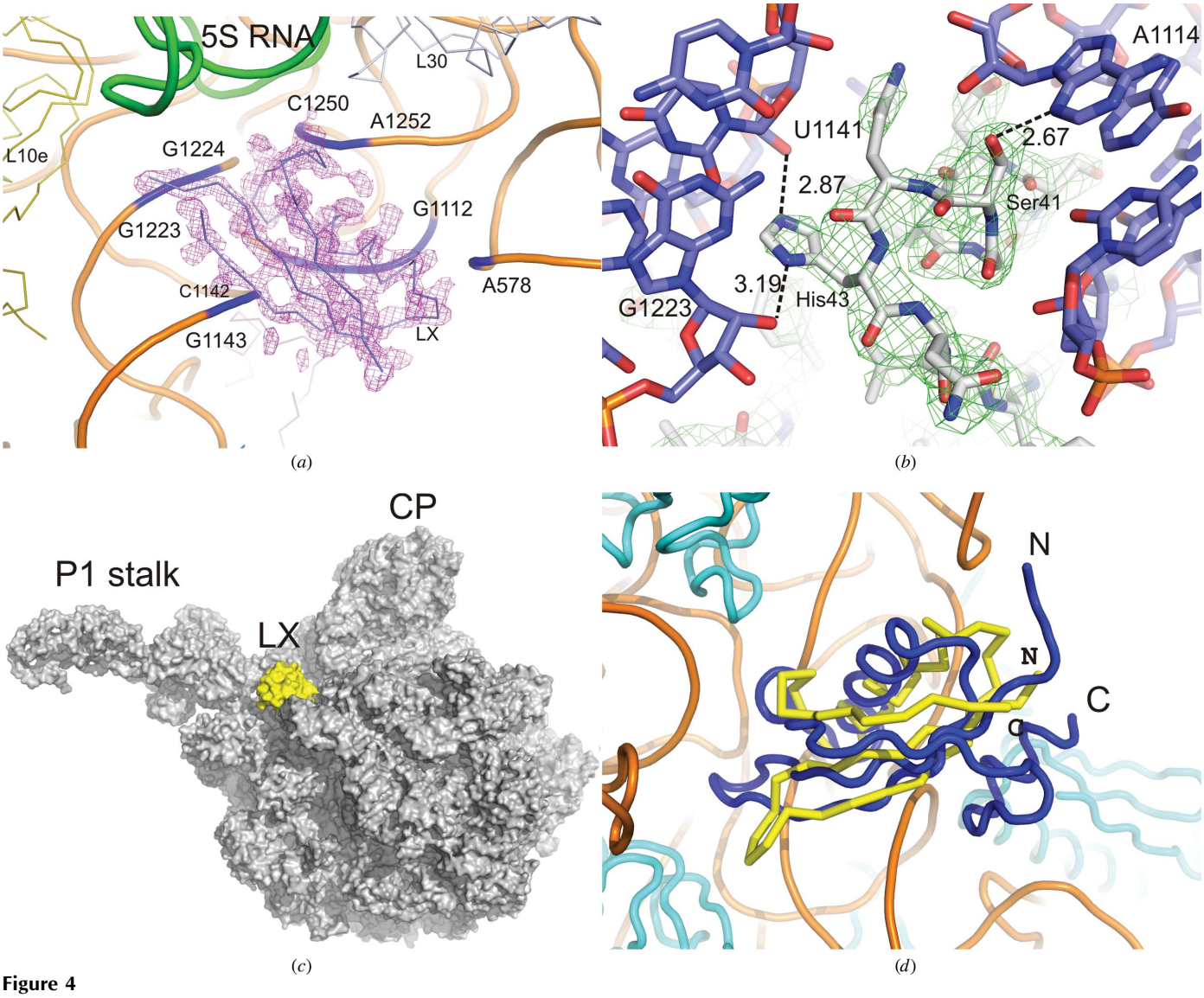

Figure 4
Structure of r-protein LX in the Hma 50S ribosomal subunit. (*a*) Electron density for r-protein LX at the 1.0σ level; the rRNA sites interacting with LX are shown in blue. (*b*) Example of electron density for a part of r-protein LX at the 1.0σ level. (*c*) Disposition of r-protein LX (yellow) in the supplemented Hma large ribosomal subunit model. (*d*) Location of the Hma LX (yellow) and Mth LX (blue) structures in the models of the Hma and *M. thermautotrophicus* 50S ribosomal subunits, respectively.

also contributes to retention of the protein within the ribosome. The surface area of the LX protein is about 4100 Å and its area of interaction with the 23S rRNA is 1046 Å (25.5% of the total surface area). The protein does not contact other r-proteins.

3.5. L1 stalk region

The L1 stalk includes 23S rRNA helices 75–78 and r-protein L1. It is a strongly conserved component of ribosomes in all domains of life. This stalk is involved in the exit of deacylated tRNA from the ribosome and was found in different relative positions in the structures of *T. thermophilus* 70S ribosome–tRNA complexes (Yusupov *et al.*, 2001; Gao *et al.*, 2009) and the isolated *D. radiodurans* 50S subunit (Harms *et al.*, 2001).

The Hma L1 stalk was modelled and incorporated by docking into a low-resolution map of the Hma 50S ribosomal subunit (Klein *et al.*, 2004), but it was not included in the deposited structure of the subunit. Our trials to find interpretable electron density for this ribosomal region in the 2.4 Å electron-density map of the Hma large ribosomal subunit led to the visualization of part of the 23S rRNA stem that belongs to the stalk (Figs. 5*a* and 5*b*). Nucleotides 2137–2149 and 2226–2237 of the 23S rRNA helix 76 could be localized.

The orientation of the presented stem corresponds to a stalk position which is intermediate between those described for the *T. thermophilus* and *D. radiodurans* ribosome structures (Fig. 5*c*; Yusupov *et al.*, 2001; Gao *et al.*, 2009; Harms *et al.*, 2001). Comparison with other available ribosome structures shows that the orientation of the Hma L1 stalk is most similar to that in structures of the *E. coli* ribosome (Schuwirth *et al.*, 2005).

3.6. Ribosomal protein L5

L5 is a strongly conserved ribosomal protein located in the central protuberance of the large subunit in ribosomes from all domains of life. It has recently been shown that knockout of the gene for r-protein L5 is lethal in *E. coli* cells (Korepanov *et al.*, 2007). On refinement of the Hma 50S ribosomal subunit structure, we could improve the original model of L5 and the adjacent site of rRNA (nucleotides 2339–2343). Loops 29–34 and 108–128 of Hma L5 have been localized (Fig. 6). Comparison of the structure of the L5 region of Hma 50S with the same region of the eukaryotic ribosome (PDB entries 3u5d and 3u5e; Ben-Shem *et al.*, 2011) demonstrates close similarity of the proteins.

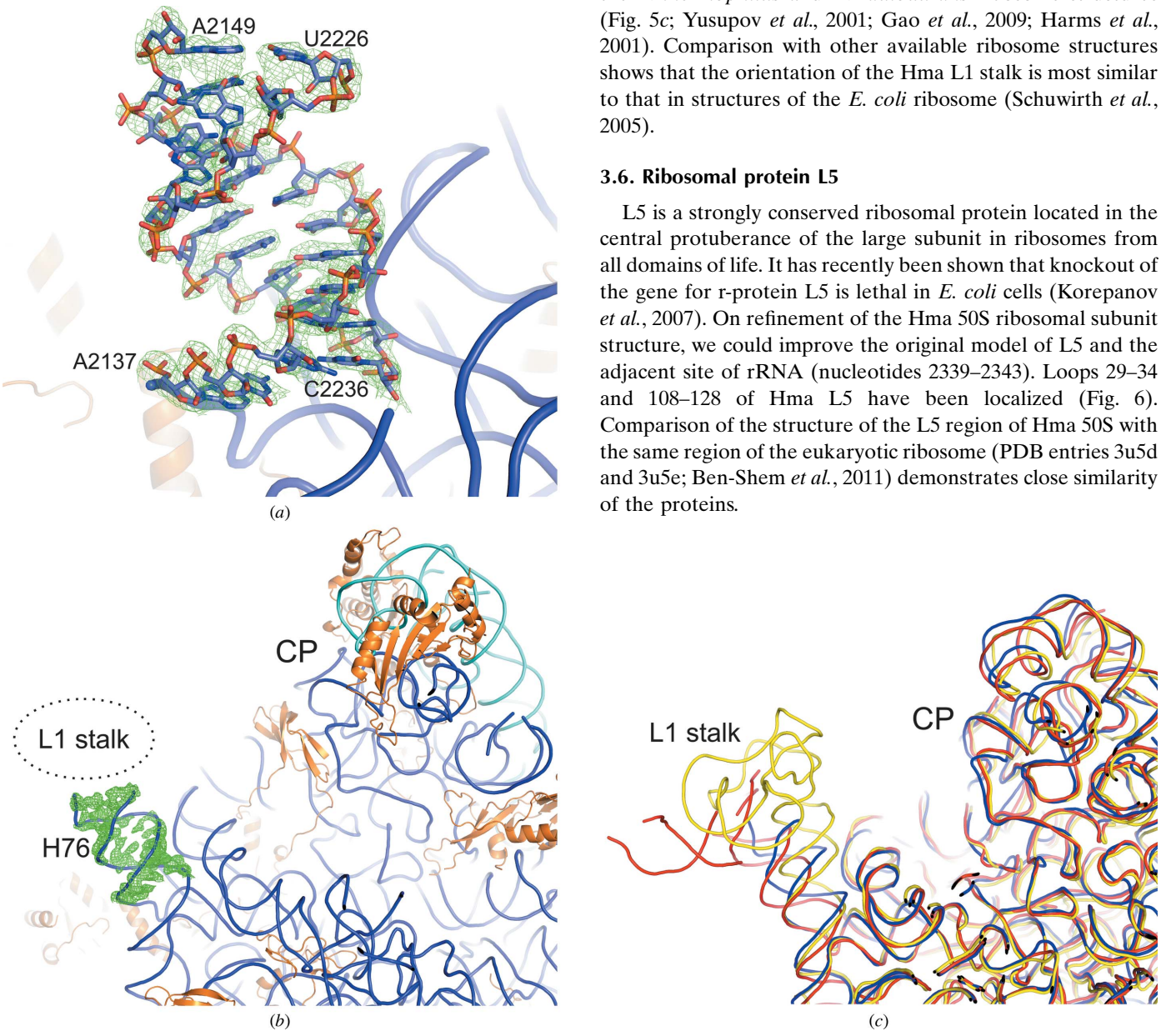

Figure 5
The present Hma large ribosomal subunit structure in the region of the L1 stalk. (*a*) The added part of H76 in the electron density at the 1.0σ level. (*b*) View of the Hma 50S subunit. (*c*) Superposition of the 23S rRNA structure of the present Hma large ribosomal subunit (blue) on the 23S rRNAs from the *T. thermophilus* ribosome (yellow; PDB entry 2wrj; Gao *et al.*, 2009) and the *D. radiodurans* 50S ribosomal subunit (red; PDB entry 1nkw; Harms *et al.*, 2001).

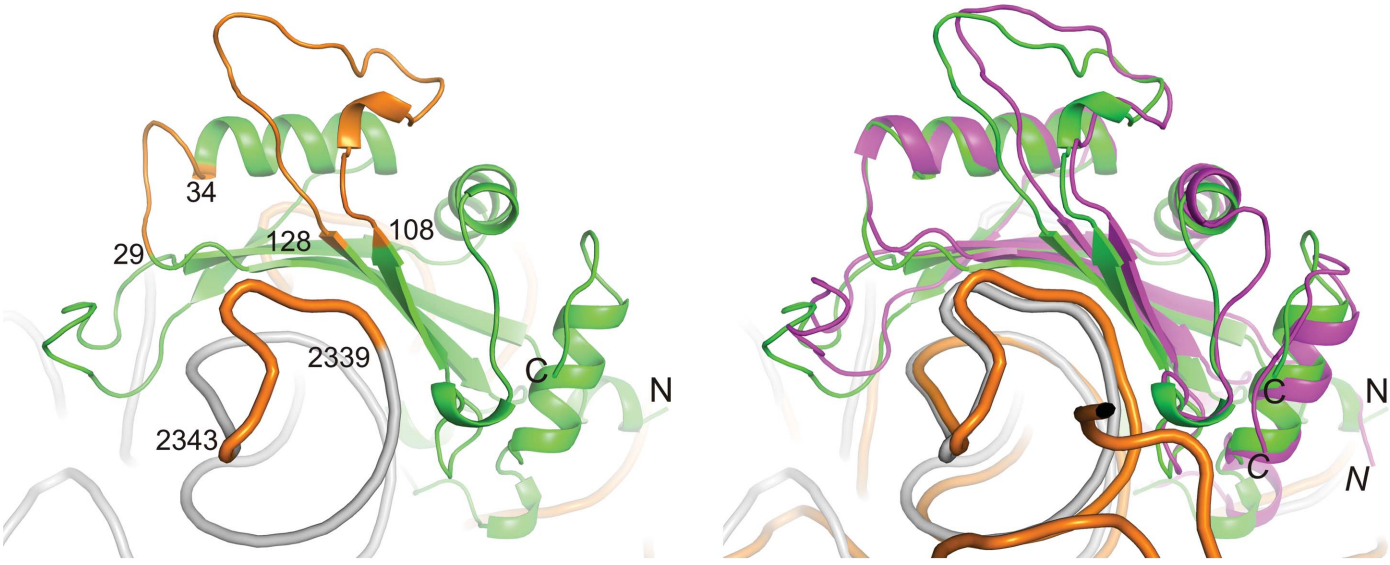

(*a*) (*b*)

Figure 6
The L5 region of the present Hma large ribosomal subunit structure. (*a*) Supplemented pieces (orange) of the L5 protein (green) and 23S RNA (grey). (*b*) Superposition of the Hma L5 (green) region on the same region (L5, magenta; rRNA, grey) of the *S. cerevisiae* ribosome (PDB entries 3u5d and 3u5e; Ben-Shem *et al.*, 2011).

4. Discussion

Archaea occupy an intermediate evolutionary position between bacteria and eukarya, but their translation system is more closely related to that of eukarya (Dennis, 1997). The sequences of the bacterial and archaeal/eukaryotic r-proteins that form the L12 or P stalks show their different natures (apart from the RNA-binding domain of L10/P0). The crystal structures of the isolated bacterial L10–L12NTD and archaeal P0–P1NTD complexes demonstrated that these proteins have different tertiary structures despite their similar domain organization. It is only recently that it has been possible to visualize the crystal structures of these highly mobile stalks within ribosomes. Firstly, the majority of the L12 ribosomal stalk was described for the 70S bacterial ribosome in complex with elongation factor G (Gao *et al.*, 2009). Some elements of the P stalk were subsequently visualized in the crystal structure of the yeast ribosome (Ben-Shem *et al.*, 2011). In this work, we revisited the crystal structure of the 50S ribosomal subunit from the halophilic archaeaon *H. marismortui* and were able to interpret electron density for a large part of r-protein P0 and for a dimer of P1 NTD bound to P0 within the archaeal ribosome. These data definitely show that the organization of the ribosomal P0 stalk is very similar in archaea and eukarya.

In the present work, the structure of the insertion domain of r-protein P0 (Kravchenko *et al.*, 2010) was visualized within the ribosome for the first time. It is probable that this domain is involved in discrimination between archaeal/eukaryotic and bacterial elongation factors. Data from an eEF2-dependent GTPase assay and on eEF2 recruitment using mutant P0 lacking domain 2 suggest that this archaeal/eukaryotic specific domain is a helper for eEF2-dependent GTPase turnover (Naganuma *et al.*, 2010). The cryo-EM structure of the 80S–eEF2 complex, in which eEF2 interacts with the P-stalk base area, also supports this suggestion (Spahn *et al.*, 2004). Incorporation of the insertion domain of P0 into the Hma 50S electron-density map and subsequent refinement led to the visualization of two C-terminal helices of this protein and one dimer of P1 NTD bound to the first C-terminal helix. Also in this work the crystal structure of the Hma LX protein within the Hma 50S ribosomal subunit is described for the first time.

Besides these two novel findings, many smaller changes have been made to improve the model of the Hma 50S ribosomal subunit. The supplemented version of the Hma 50S ribosomal subunit model (PDB entries 4hub and 4i4m) contains 103 846 non-H atoms. The structure includes 2808 nucleotides of the 2922 nucleotides in the 23S RNA compared with 2754 in the initial structure (PDB entry 3cc2), all of the 122 nucleotides in the 5S RNA and 4311 (compared with 3775) amino-acid residues from 32 (compared with 29) ribosomal proteins, as well as 261 (compared with 209) ions (138 Mg^{2+}, 30 Cl^{-}, 85 Na^{+}, three K^{+} and five Cd^{2+}) and 7745 (compared with 7823) water molecules. The structure has been refined to an R factor of 16.56% (compared with 19.9%) and an R_{free} of 20.62% (compared with 23.1%).

This work was supported by the Russian Academy of Sciences (RAS), the Russian Foundation for Basic Research (11-04-00327-a) and the Program of the RAS on Molecular and Cellular Biology.

References

Afonine, P. V., Grosse-Kunstleve, R. W., Echols, N., Headd, J. J., Moriarty, N. W., Mustyakimov, M., Terwilliger, T. C., Urzhumtsev, A., Zwart, P. H. & Adams, P. D. (2012). *Acta Cryst.* D**68**, 352–367.
Ban, N., Nissen, P., Hansen, J., Moore, P. B. & Steitz, T. A. (2000). *Science*, **289**, 905–920.
Ben-Shem, A., Garreau de Loubresse, N., Melnikov, S., Jenner, L., Yusupova, G. & Yusupov, M. (2011). *Science*, **334**, 1524–1529.

Blaha, G., Gürel, G., Schroeder, S. J., Moore, P. B. & Steitz, T. A. (2008). *J. Mol. Biol.* **379**, 505–519.
Dennis, P. P. (1997). *Cell*, **89**, 1007–1010.
Diaconu, M., Kothe, U., Schlünzen, F., Fischer, N., Harms, J. M., Tonevitsky, A. G., Stark, H., Rodnina, M. V. & Wahl, M. C. (2005). *Cell*, **121**, 991–1004.
Emsley, P., Lohkamp, B., Scott, W. G. & Cowtan, K. (2010). *Acta Cryst.* D**66**, 486–501.
Gao, Y.-G., Selmer, M., Dunham, C. M., Weixlbaumer, A., Kelley, A. C. & Ramakrishnan, V. (2009). *Science*, **326**, 694–699.
Greber, B. J., Boehringer, D., Godinic-Mikulcic, V., Crnkovic, A., Ibba, M., Weygand-Durasevic, I. & Ban, N. (2012). *J. Mol. Biol.* **418**, 145–160.
Harms, J., Schluenzen, F., Zarivach, R., Bashan, A., Gat, S., Agmon, I., Bartels, H., Franceschi, F. & Yonath, A. (2001). *Cell*, **107**, 679–688.
Holm, L. & Rosenström, P. (2010). *Nucleic Acids Res.* **38**, W545–W549.
Hooft, R. W., Vriend, G., Sander, C. & Abola, E. E. (1996). *Nature (London)*, **381**, 272.
Kavran, J. M. & Steitz, T. A. (2007). *J. Mol. Biol.* **371**, 1047–1059.
Klein, D. J., Moore, P. B. & Steitz, T. A. (2004). *J. Mol. Biol.* **340**, 141–177.
Klinge, S., Voigts-Hoffmann, F., Leibundgut, M., Arpagaus, S. & Ban, N. (2011). *Science*, **334**, 941–948.
Korepanov, A. P., Gongadze, G. M., Garber, M. B., Court, D. L. & Bubunenko, M. G. (2007). *J. Mol. Biol.* **366**, 1199–1208.
Kravchenko, O., Mitroshin, I., Nikonov, S., Piendl, W. & Garber, M. (2010). *J. Mol. Biol.* **399**, 214–220.
Laskowski, R. A., MacArthur, M. W., Moss, D. S. & Thornton, J. M. (1993). *J. Appl. Cryst.* **26**, 283–291.
Möller, W. & Maassen, J. A. (1986). *Structure, Function, and Genetics of Ribosomes*, edited by B. Hardesty & G. Kramer, pp. 309–325. New York: Springer-Verlag.
Murshudov, G. N., Skubák, P., Lebedev, A. A., Pannu, N. S., Steiner, R. A., Nicholls, R. A., Winn, M. D., Long, F. & Vagin, A. A. (2011). *Acta Cryst.* D**67**, 355–367.
Naganuma, T., Nomura, N., Yao, M., Mochizuki, M., Uchiumi, T. & Tanaka, I. (2010). *J. Biol. Chem.* **285**, 4747–4756.
Nomura, T., Nakano, K., Maki, Y., Naganuma, T., Nakashima, T., Tanaka, I., Kimura, M., Hachimori, A. & Uchiumi, T. (2006). *Biochem. J.* **396**, 565–571.
Schuwirth, B. S., Borovinskaya, M. A., Hau, C. W., Zhang, W., Vila-Sanjurjo, A., Holton, J. M. & Cate, J. H. D. (2005). *Science*, **310**, 827–834.
Spahn, C. M., Gomez-Lorenzo, M. G., Grassucci, R. A., Jørgensen, R., Andersen, G. R., Beckmann, R., Penczek, P. A., Ballesta, J. P. & Frank, J. (2004). *EMBO J.* **23**, 1008–1019.
Uchiumi, T., Honma, S., Nomura, T., Dabbs, E. R. & Hachimori, A. (2002). *J. Biol. Chem.* **277**, 3857–3862.
Yusupov, M. M., Yusupova, G. Z., Baucom, A., Lieberman, K., Earnest, T. N., Cate, J. H. D. & Noller, H. F. (2001). *Science*, **292**, 883–896.
Zimmermann, R. A. (1980). *Ribosomes. Structure, Function and Genetics*, edited by G. Chambliss, G. R. Craven, J. Davies, K. Davis, L. Kahan & M. Nomura, pp. 135–169. Baltimore: University Park Press.